UMT PRESS
Journal of Mathematical Sciences and Informatics
Journal Homepage: https://journal.umt.edu.my/index.php/jmsi
eISSN: 2948-3697
DOI: http://doi.org/10.46754/jmsi.2026.06.003

PHYSICS-INFORMED NEURAL NETWORKS MODIFICATION FOR SOLVING 2D SHALLOW WATER EQUATIONS

NURSYIVA IRSALINDA[1,2], MAHARANI ABU BAKAR[1]* AND NORIZAN MOHAMED[1]

[1]Faculty of Computer Science and Mathematics, Universiti Malaysia Terengganu, 21030 Kuala Nerus, Terengganu, Malaysia. [2]Faculty of Science and Applied Technology, Universitas Ahmad Dahlan, Banguntapan 55191, Bantul, Yogyakarta, Indonesia.

**Corresponding author: maharani@umt.edu.my*

ARTICLE INFO

Article History:
Received: 20 November 2025
Revised: 19 December 2025
Accepted: 5 March 2026
Published: 15 June 2026

Keywords:
dynamic strategy, finite difference method, mesh refinement, Physics-Informed Neural Networks (PINN), 2D shallow water equations.

ABSTRACT

This study investigates the use of Physics-Informed Neural Networks (PINN) for solving the two-dimensional shallow water equations (SWE) on a flat bed and proposes a modified PINN with dynamic mesh-refinement strategy that adaptively increases the density of collocation points in critical or stiff regions such as propagating wave fronts and rapidly varying gradients. In the proposed framework, shallow-water physics is enforced as soft constraints in the loss, with initial and boundary conditions embedded to ensure a well-posed formulation without labelled targets. We evaluated fully connected architectures using the Adaptive Moment Estimation (Adam) and Limited-memory Broyden–Fletcher–Goldfarb–Shanno (L-BFGS) optimisation algorithms. Fully connected neural networks are trained using a combination of Adam and L-BFGS optimisers, and a FDM solution is employed as a reference for quantitative comparison. The standard PINN and its dynamically refined variant are evaluated against the FDM benchmark in terms of convergence behaviour and predictive accuracy. The results show that the refined PINN concentrates collocation points in stiff regions, reduces errors near wave fronts, and achieves accuracy closer to FDM with faster convergence.

2020 Mathematics Subject Classification:

Introduction

Accurate modelling of shallow-water wave behaviour is essential for applications such as flood risk assessment, navigation safety, and coastal infrastructure planning [1, 2]. In realistic settings, wave fields often develop sharp fronts, dispersive features, and multi-scale nonlinear interactions that challenge classical numerical discretisation's and substantially increase computational cost when fine spatial resolution is required. Although finite difference and finite element methods, as well as spectral models, remain the backbone of operational prediction, their performance can deteriorate under such conditions, particularly when steep

gradients and nonlinear interactions must be resolved or when simplifying modelling assumptions introduce additional uncertainties [3, 4, 5, 6].

Physics-Informed Neural Networks (PINNs) have recently emerged as mesh-free alternatives for solving partial differential equations (PDEs) by learning continuous solution fields through the enforcement of governing equations, initial conditions, and boundary conditions within a unified loss function [7, 8, 9]. While PINNs reduce dependence on labelled data and offer smooth, differentiable representations, their performance can deteriorate for stiff or multi-scale shallow-water flows, where uniform collocation sampling struggles to resolve steep gradients. Recent efforts addressing this limitation include adaptive sampling, domain decomposition, and hybrid optimisation strategies combining Adam and L-BFGS [10, 11, 12, 13].

In this study, we investigate PINNs for the two-dimensional shallow water equations on a flat bed and propose a dynamically refined collocation strategy that increases point density in stiff regions, particularly near propagating wave fronts. The method enforces shallow-water physics as soft constraints and incorporates initial and boundary conditions, enabling training without reference solution data. Fully connected architectures, with optional Fourier feature embeddings, are optimised using the Adam and then the L-BFGS algorithms.

An FDM solution is employed as a benchmark for quantitative evaluation [14]. We compare a standard PINN and the dynamically refined PINN on canonical 2D-SWE test cases using error metrics including relative L^2 error, and convergence behaviour, as characterised by loss evolution over training iterations [15]. This work aims to clarify when dynamic refinement enhances PINN accuracy and convergence relative to a baseline PINN, while preserving a smooth and differentiable representation suitable for further analysis and downstream applications.

Preliminaries

This section provides the theoretical background for the proposed method, including the formulation of the two-dimensional shallow water equations and the fundamentals of the physics-informed neural network framework.

Two-Dimensional Shallow Water Equations

The Two-Dimensional Shallow Water Equations (2D-SWE) constitute a fundamental system of partial differential equations that model the behaviour of incompressible, hydrostatic, and free-surface flows in shallow regions. These equations are particularly appropriate when the characteristic water depth is significantly smaller than the horizontal length scales, which is typical in coastal, estuarine, riverine, and floodplain, environments [16, 17].

Mathematically, the 2D-SWE captures the conservation of mass (continuity) and the conservation of momentum in both horizontal directions. The continuity equation expresses the balance of water volume, while the momentum equations account for the horizontal transport of momentum, gravitational acceleration, and the influence of bathymetric variations. The standard form of the 2D-SWE is given by:

$$\begin{aligned}
&\frac{\partial h}{\partial t}+\frac{\partial (hu)}{\partial x}+\frac{\partial (hv)}{\partial y}=0\\
&\frac{\partial (hu)}{\partial t}+\frac{\partial}{\partial x}\left(hu^2+\frac{1}{2}gh^2\right)+\frac{\partial (huv)}{\partial y}=-gh\frac{\partial b}{\partial x}\\
&\frac{\partial (hv)}{\partial t}+\frac{\partial (huv)}{\partial x}+\frac{\partial}{\partial y}\left(hv^2+\frac{1}{2}gh^2\right)=-gh\frac{\partial b}{\partial y}
\end{aligned} \tag{1}$$

where $h(x,y,t)$ denotes the water surface elevation measured from the bathymetric baseline, $u(x,y,t)$ and $v(x,y,t)$ represent the horizontal velocity components in the x and y directions, respectively, whereas $b(x,y)$ is the bathymetric profile (bottom topography), and g is the gravitational acceleration constant.

Physically, these equations account for several key processes. They represent the advection of momentum, which describes the transport of water mass and momentum through its own velocity field. Additionally, they incorporate hydrostatic pressure gradients, approximated by the terms involving $\frac{1}{2}gh^2$, which reflect the distribution of pressure due to the water column. Finally, they include topographic forcing, where gradients in the bathymetry introduce source terms in the momentum equations, capturing the effects of variations in the underlying bottom topography on the overall flow dynamics.

Physics Informed Neural Networks

Physics-Informed Neural Networks (PINNs) are an advanced Artificial Neural Network (ANN) approach that effectively addresses unsupervised learning tasks. By embedding the governing Partial Differential Equations (PDEs) directly into its loss function as a form of regularisation, the PINN is able to integrate and respect the underlying physical laws of the modelled system [18, 19, 20]. Based on Equation (1), this study generated an ANN architecture of PINN as presented in Figure 1.

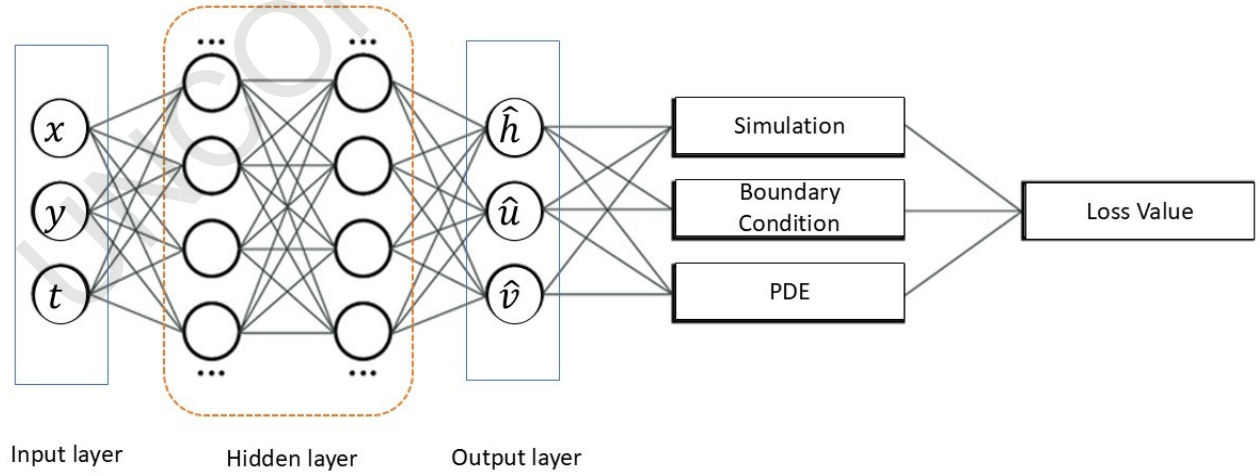

Figure 1: The PINN architecture for 2D-SWEs

Based on Equation (1), this research paper aims to determine three depth-averaged state variables that describe the system's evolution over space and time:

$$(h, u, v): (x, y, t) \to \mathbb{R}^3,$$

approximated by a neural network:

$$(h_\theta, u_\theta, v_\theta) = \mathcal{N}_\theta(x, y, t),$$

where θ denotes trainable parameters. Spatial and temporal derivatives are obtained by Automatic Differentiation (AD). By replacing (h, u, v) with the neural network predictions in the conservative 2D-SWE in Equation (1), we obtain the associated PDE residual terms as follows:

$$\begin{aligned} \mathcal{R}_1 &= \partial_t h_\theta + \partial_x(h_\theta u_\theta) + \partial_y(h_\theta v_\theta), \\ \mathcal{R}_2 &= \partial_t(h_\theta u_\theta) + \partial_x\left(h_\theta u_\theta^2 + \frac{1}{2} g h_\theta^2\right) + \partial_y(h_\theta u_\theta v_\theta) + g h_\theta \partial_x b, \\ \mathcal{R}_3 &= \partial_t(h_\theta v_\theta) + \partial_x(h_\theta u_\theta v_\theta) + \partial_y\left(h_\theta v_\theta^2 + \frac{1}{2} g h_\theta^2\right) + g h_\theta \partial_y b. \end{aligned} \tag{2}$$

To train the PINN model, three sets of collocation points had been defined. The set $S_r = \{(x_i, y_i, t_i)\}_{i=1}^{N_r}$ contains the interior collocation points used to enforce the PDEs. The set $S_0 = \{(x_j, y_j, 0)\}_{j=1}^{N_0}$ represents the initial-condition (IC) points, while the set $S_b = \{(x_k, y_k, t_k)\}_{k=1}^{N_b}$ corresponds to the boundary-condition (BC) points, which can be periodic, solid-wall, or open depending on the problem setup.

The total loss function combines contributions from the PDE residuals and the boundary and initial conditions. The PDE residual loss, $\mathcal{L}_{PDE}$ measures the mean-squared violation of the governing equations at the collocation points, where each residual $\mathcal{R}_1$ corresponds to the continuity and momentum equations of the 2D shallow-water system. It is expressed as:

$$\mathcal{L}_{PDE} = \frac{1}{N_r} \sum_{S_r} (\mathcal{R}_1^2 + \mathcal{R}_2^2 + \mathcal{R}_3^2).$$

In addition, the initial-condition loss, $\mathcal{L}_{IC}$ ensures that the network predictions satisfy the prescribed initial values of water height and velocity fields. It is formulated as:

$$\mathcal{L}_{IC} = \frac{1}{N_0} \sum_{S_0} (|h_\theta - h_0|^2 + |u_\theta - u_0|^2 + |v_\theta - v_0|^2),$$

where h_0, u_0 and v_0 denote initial conditions. The boundary-condition loss $\mathcal{L}_{BC}$, ensures that the neural network predictions satisfy the physical constraints imposed along the boundaries of the computational domain. To represent different types of boundary conditions in a unified form, an operator $\Phi(.)$ is introduced. This operator encodes the specific boundary condition applied at each boundary point. Mathematically, the boundary-condition loss is formulated as:

$$\mathcal{L}_{BC} = \frac{1}{N_b}\sum_{S_b} \|\Phi(h_\theta u_\theta v_\theta; x, y, t)\|^2.$$

By minimising the total loss, $\mathcal{L}_{BC}$, the PINN framework enforces that the learned solution conforms to the required physical boundary behaviours throughout the training process. For PINN cycle the total loss is expressed as:

$$\mathcal{L}_{total} = \mathcal{L}_{PDE} + \mathcal{L}_{IC} + \mathcal{L}_{BC}.$$

Through minimisation of $\mathcal{L}_{total}$, the neural network learns a continuous, differentiable approximation of the shallow-water solution that is consistent with both the physical laws and the prescribed initial and boundary conditions.

Methodology

This subsection presents the dynamic mesh refinement strategy employed in this study, detailing how collocation points are adaptively updated during training to better resolve stiff regions in the solution of the 2D shallow water equations.

Dynamic Mesh Refinement Strategy for PINNs

Dynamic mesh refinement introduces an adaptive sampling strategy that increases the density of collocation points in regions exhibiting sharp gradients or rapid solution variations. Let $\Omega = [0,1] \times [0,1]$ represent the spatial domain used to solve the two-dimensional PDE. Within this domain, two types of grids are introduced as a training domain and a refined (dummy) domain. The training domain, Ω_t covers the entire region with a coarser grid resolution to capture the overall behaviour of the solution efficiently.

In contrast, the refined domain Ω_t focuses on smaller localised areas where the solution exhibits sharp gradients or rapid variations. This refined domain uses a finer grid spacing to improve learning accuracy in regions of high stiffness. By combining both domains, the model maintains computational efficiency across smooth regions while improving resolution and stability in areas with strong variations, leading to a balanced and accurate representation of the 2D PDE solution. Figure 2 illustrates the training and refined (dummy) domains in two dimensions, along with their integration for solving the 2D-SWE using the PINN framework.

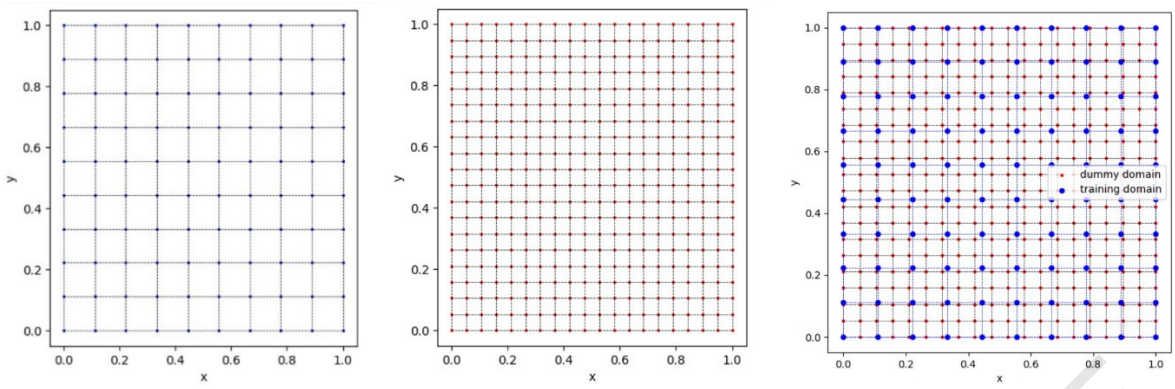

(a) Training domain (b) Dummy domain (c) Combined domain

Figure 2: An illustration of (a) the training domain, (b) the refined domain, and (c) their integration for solving the 2D-SWE using the dynamic mesh refinement strategy within the PINN framework

The process begins by training the standard PINN on an initial set of randomly sampled collocation points, referred to as the training domain Ω_t. After several training iterations, the predicted solutions $(h_\theta, u_\theta, v_\theta) = \mathcal{N}_\theta(x, y, t)$ are analysed to detect regions exhibiting high gradient or curvature magnitudes, which correspond to dynamically evolving stiff zones within the domain.

First, the gradient magnitude of the solution is computed using automatic differentiation as follows:

$$G(x, y, t) = \|\nabla u_\theta(x, y, t)\| = \sqrt{\left(\frac{\partial u_\theta}{\partial x}\right)^2 + \left(\frac{\partial u_\theta}{\partial y}\right)^2}.$$

A subset of points exceeding a prescribed gradient threshold τ_G is then identified as:

$$\Omega_G = \{(x, y) \in \Omega_t | G(x, y, t) > \tau_G\}.$$

To further refine regions where the solution exhibits rapid curvature changes, the second-order derivatives are evaluated as follows:

$$C(x, y, t) = \max\left(\left|\frac{\partial^2 u_\theta}{\partial x^2}\right|, \left|\frac{\partial^2 u_\theta}{\partial y^2}\right|\right).$$

Points with curvature exceeding the threshold τ_C are marked as:

$$\Omega_C = \{(x, y) \in \Omega_t | C(x, y, t) > \tau_C\}.$$

The refined (dummy) domain Ω_d is then constructed as the union of these detected regions:

$$\Omega_d = \Omega_G \cup \Omega_C$$

New collocation points are sampled densely within Ω_d, effectively increasing the training-point density in critical regions. The updated training set after refinement is given by:

$$\Omega_t{}^{(k+1)} = \Omega_t{}^{(k)} + \Omega_d{}^{(k)},$$

where k is the number of cycle in a certain iteration.

The adaptive enrichment procedure described above is not only heuristic but also supported by theoretical insights from residual-based refinement strategies in physics-informed learning. In particular, allocating new collocation points in regions of large gradients or curvature effectively reduces the local residual, which in turn accelerates the convergence of the global PINN approximation.

Flowchart Dynamic Mesh Refinement for PINNs

The flowchart in Figure 3 summarises the algorithmic workflow of the dynamic mesh refinement strategy for PINNs, highlighting how collocation points are adaptively refined based on the evolving solution behaviour.

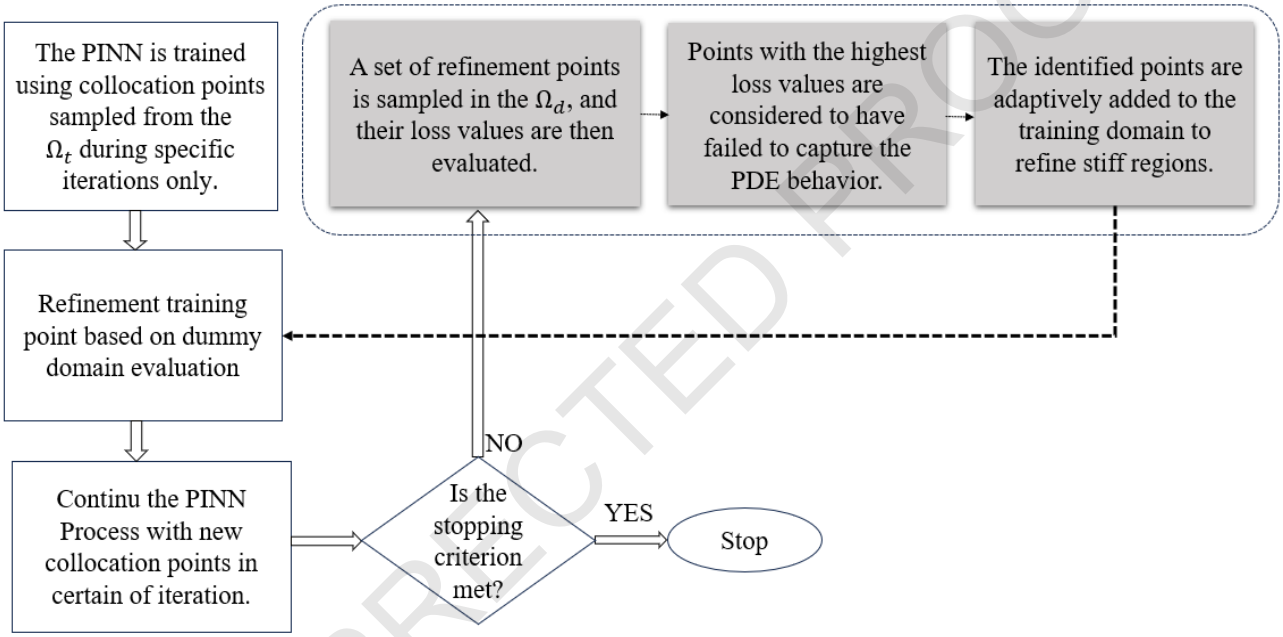

Figure 3: Algorithmic workflow of the proposed dynamic mesh refinement strategy for PINNs, including loss-based evaluation of candidate points, adaptive collocation point enrichment, and iterative training until convergence

Experimental Results

In this section, solutions obtained using a standard PINN and a dynamically refined PINN are compared with a high-resolution reference solution computed using the FDM. Within the PINN framework, the trainable parameter vector θ represents all weights and biases of the neural network that approximates the state-variable fields of the 2D-SWE.

Given the spatio-temporal coordinates (x, y, t), the neural network outputs the surrogate predictions $\hat{h}(x, y, t; \theta)$, $\hat{u}(x, y, t; \theta)$, and $\hat{v}(x, y, t; \theta)$, corresponding to the water depth and the horizontal velocity components. These surrogate fields are then substituted into the governing 2D-SWE to construct the physics-based residuals, which quantify how well the network predictions satisfy the governing equations.

Specifically, the continuity equation residual is defined as:

$$r_h(x,y,t;\theta) = \frac{\partial \hat{h}}{\partial t}(x,y,t;\theta) + \frac{\partial}{\partial x}\left(\hat{h}\hat{u}\right)(x,y,t;\theta) + \frac{\partial}{\partial y}\left(\hat{h}\hat{v}\right)(x,y,t;\theta),$$

while the residuals corresponding to the momentum conservation in the x and y directions are given by:

$$r_u(x,y,t;\theta) = \frac{\partial \hat{h}}{\partial t}(x,y,t;\theta) + \frac{\partial}{\partial x}\left(\hat{h}\hat{u}^2 + \frac{1}{2}g\hat{h}^2\right)(x,y,t;\theta) + \frac{\partial}{\partial y}\left(\hat{h}\hat{u}\hat{v}\right)(x,y,t;\theta),$$

$$r_v(x,y,t;\theta) = \frac{\partial \hat{h}}{\partial t}(x,y,t;\theta) + \frac{\partial}{\partial x}\left(\hat{h}\hat{u}\hat{v}\right)(x,y,t;\theta) + \frac{\partial}{\partial y}\left(\hat{h}\hat{v}^2 + \frac{1}{2}g\hat{h}^2\right)(x,y,t;\theta).$$

Based on these residual expressions, the loss function for the 2D Shallow Water Equations is formulated by combining the PDE loss, boundary condition loss, and initial condition loss. Let $\left(x_f^{(i)}, y_f^{(i)}, t_f^{(i)}\right)$ denote the interior collocation points. The PDE loss is then defined as

$$\mathcal{L}_{PDE}(\theta) = \frac{1}{N_f}\sum_{i=1}^{N_f}\left(\left|r_h^{(i)}(\theta)\right|^2 + \left|r_u^{(i)}(\theta)\right|^2 + \left|r_v^{(i)}(\theta)\right|^2\right).$$

The loss component associated with the initial conditions enforces the network predictions at time $t = 0$, such that:

$$h(x,y,0) = h_0(x,y), \quad u(x,y,0) = u_0(x,y), \quad v(x,y,0) = v_0(x,y).$$

Let$\left(x_{IC}^{(i)}, y_{IC}^{(i)}, 0\right)$ denote the initial condition points. The initial condition loss is formulated as follows:

$$\mathcal{L}_{IC}(\theta) = \frac{1}{N_{IC}}\sum_{i=1}^{N_{IC}}\left(\left|\hat{h}\left(x_{IC}^{(i)}, y_{IC}^{(i)}, 0;\theta\right) - h_0^{(i)}\right|^2 + \left|\hat{u}\left(x_{IC}^{(i)}, y_{IC}^{(i)}, 0;\theta\right) - u_0^{(i)}\right|^2 + \left|\hat{v}\left(x_{IC}^{(i)}, y_{IC}^{(i)}, 0;\theta\right) - v_0^{(i)}\right|^2\right).$$

Similarly, the boundary condition loss is defined at boundary points $\left(x_{BC}^{(i)}, y_{BC}^{(i)}, t_{BC}^{(i)}\right)$ with prescribed target values $h_{BC}^{(i)}$, $u_{BC}^{(i)}$ and $v_{BC}^{(i)}$ as:

$$\mathcal{L}_{BC}(\theta) = \frac{1}{N_{BC}}\sum_{i=1}^{N_{BC}}\left(\left|\hat{h}\left(x_{BC}^{(i)}, y_{BC}^{(i)}, t_{BC}^{(i)};\theta\right) - h_{BC}^{(i)}\right|^2 + \left|\hat{u}\left(x_{BC}^{(i)}, y_{BC}^{(i)}, t_{BC}^{(i)};\theta\right) - u_{BC}^{(i)}\right|^2 + \left|\hat{v}\left(x_{BC}^{(i)}, y_{BC}^{(i)}, t_{BC}^{(i)};\theta\right) - v_{BC}^{(i)}\right|^2\right).$$

The overall training objective is defined by combining the 2D-SWE residual loss with the initial and boundary condition losses, resulting in the total loss function. The total loss is written as:

$$\mathcal{L}(\theta) = \mathcal{L}_{PDE}(\theta) + \mathcal{L}_{IC}(\theta) + \mathcal{L}_{BC}(\theta).$$

Loss Convergence and Iterative Behaviour

This subsection examines the iterative behaviour of the PINN models through the evolution of the loss function. A PINN architecture with three hidden layers of 64 neurons each is employed, using 2,000 interior collocation points, 200 initial condition points, and 200 boundary condition points.

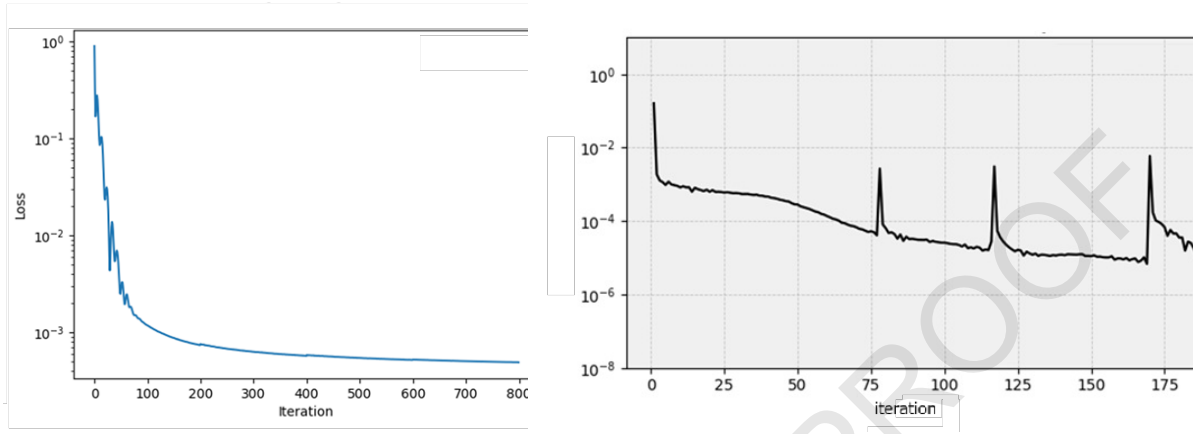

(a) (b)

Figure 4: Loss value comparison between (a) PINN and (b) PINN with dynamic mesh refinement

As illustrated in Figure 4, with the same configurations the PINN with dynamic mesh refinement achieves a lower loss compared to the standard PINN. In the dynamically refined PINN, the loss function exhibits a rise at the beginning of each refinement cycle, followed by a further decrease, with each cycle reaching a lower loss level than the previous one. Under a maximum of 1,000 training iterations, the refined PINN attains a minimum loss of the order of 10^{-6} after only about 230 iterations, whereas the standard PINN converges around iteration 800 with a minimum loss of approximately 10^{-4}. These numerical results indicate that the dynamic mesh refinement strategy improves efficiency in terms of the required number of iterations" and the overall reduction in the loss value.

Accuracy and Error Analysis

To assess model performance, the predicted solution fields are compared with the FDM reference solution for the 2D-SWE at three representative time instances, as illustrated in Figure 5.

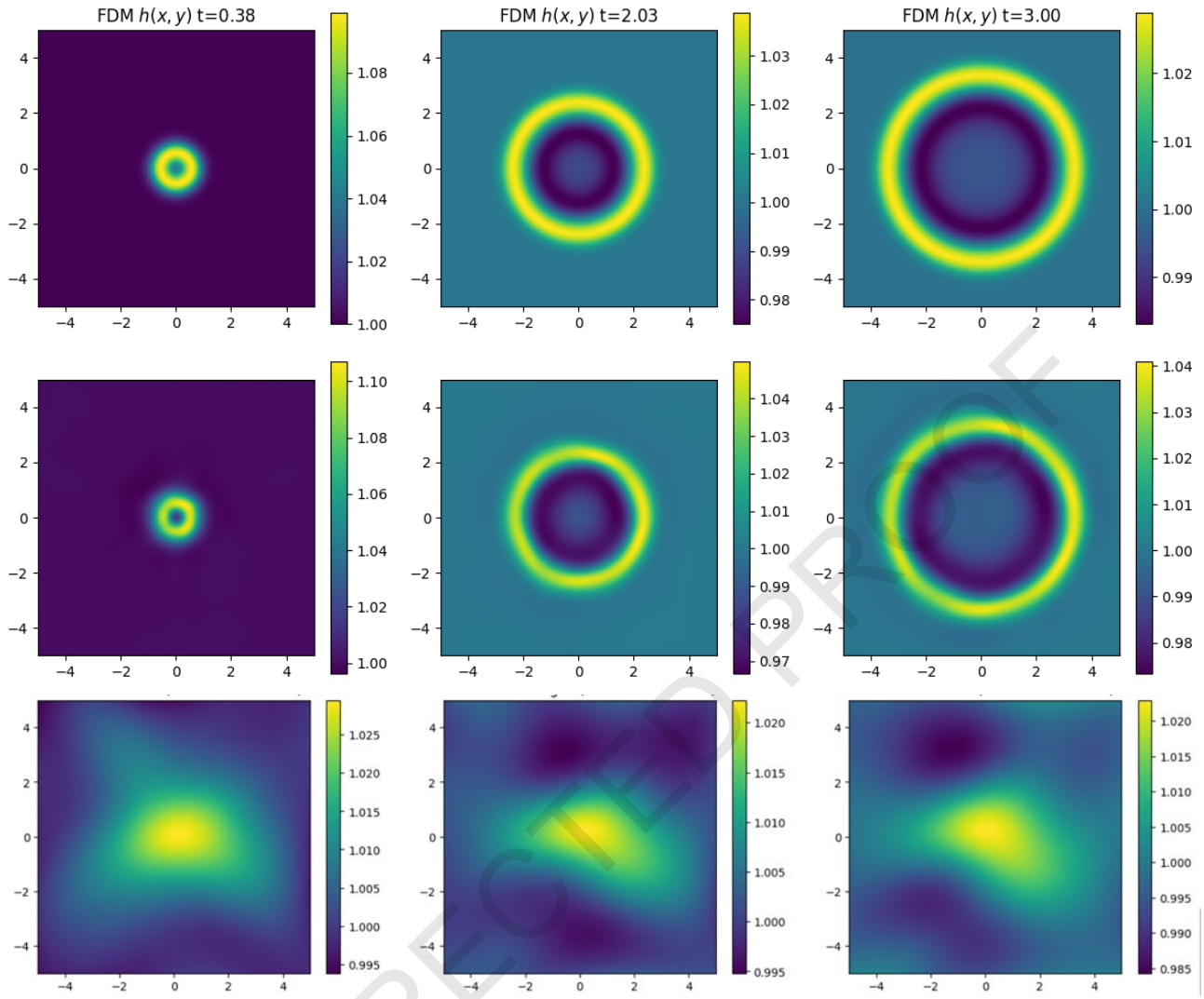

Figure 5: Spatial solution fields of the 2D-SWE predicted by the FDM (top row), dynamically refined PINN (middle row), and baseline PINN (bottom row), illustrating differences in wave-front resolution

From Figure 5, it is evident that the PINN with the dynamic mesh refinement strategy produces predictions that more closely match the FDM reference solution, which serves as the numerical benchmark in this study. This observation is consistent with the earlier findings regarding the lower loss values achieved by the refined PINN model. Furthermore, the comparison between solution profiles in several temporal slices in Figures 6 and 7 demonstrates that the PINN incorporating dynamic mesh refinement yields results that closely replicates the reference solution.

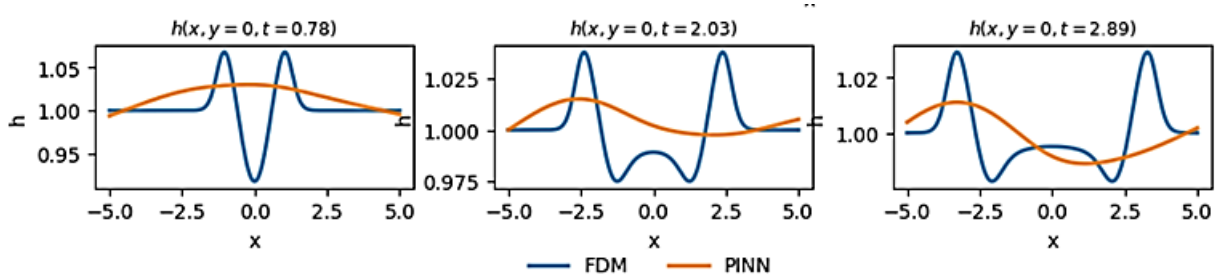

Figure 6: Comparison of prediction solutions of 2D-SWE obtained by PINN at several temporal slices

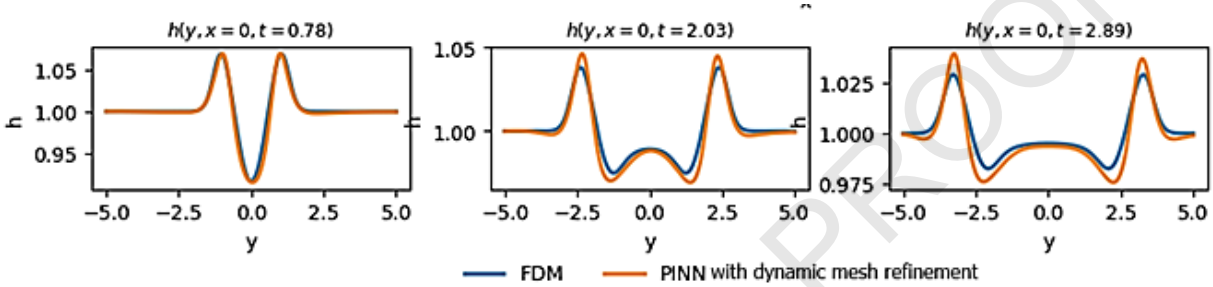

Figure 7: Comparison of prediction solutions of 2D-SWE obtained by PINN with dynamic mesh refinement at several temporal slices

The absolute error produced by each method is also examined, as presented in the heatmap visualisation in Figure 8 and the numerical summary in Table 1.

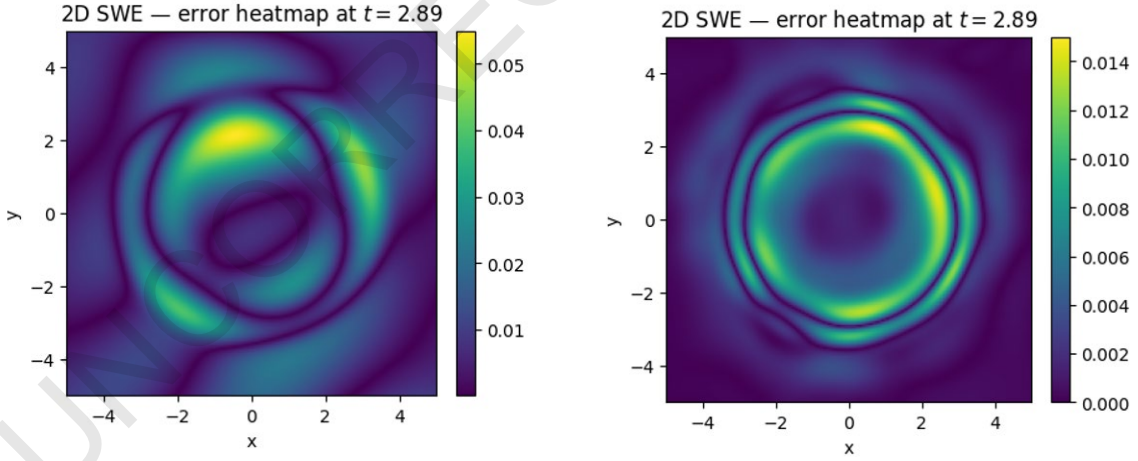

(a) (b)

Figure 8: Absolute error of solution 2D-SWE obtained by (a) PINN and (b) PINN with dynamic mesh refinement

Table 1: Experimental results of 2D-SWE

Method	Iteration	Loss Value	Absolute Error
PINN	800	1,259435e-04	1.208862e-02
PINN with dynamic mesh refinement	230	2,356221e-06	3,187631e-04

Based on these results, it is evident that the absolute error generated by the PINN with dynamic mesh refinement is significantly lower than that of the standard PINN.

Discussion

The numerical experiments demonstrate that incorporating a dynamic mesh refinement strategy into the PINN framework significantly improves model accuracy and training efficiency for solving 2D-SWE. Compared with the baseline PINN, which converges more slowly and stabilises at a higher loss level, the dynamically refined PINN consistently attains lower loss values across successive refinement cycles, resulting in closer quantitative and qualitative agreement with the FDM reference solution.

The benefits of dynamic refinement are evident in the predicted water depth and velocity fields at multiple time instances, where sharper wave fronts and smoother transitions are more accurately resolved. Slice-based comparisons further confirm that the refined PINN produces solution structures that are nearly indistinguishable from the FDM benchmark, indicating superior spatial-temporal resolution. This observation is reinforced by the absolute error heatmaps and numerical summaries, which show substantially reduced error magnitudes across the computational domain.

Despite these advantages, the proposed refinement strategy also introduces certain limitations. In particular, the adaptive enrichment of collocation points increases the training complexity and may lead to higher computational overhead if refinement is applied too frequently or without appropriate stopping criteria. Moreover, for problems with extremely complex or rapidly evolving stiffness patterns, the effectiveness of loss-based refinement may depend on the choice of refinement thresholds and sampling strategies. Addressing these aspects, for example through automated refinement control or hybrid error indicators, represents an important direction for future work.

Overall, these results indicate that dynamic mesh refinement enables PINNs to more efficiently allocate collocation points in regions of higher solution complexity, thereby improving numerical stability, convergence behaviour, and predictive fidelity. As such, dynamic refinement constitutes a promising extension of the PINN framework for nonlinear hyperbolic systems such as the 2D shallow water equations.

Conclusion

This study presents a comparative investigation of the standard PINN and a dynamically refined PINN for solving the 2D-SWE, using a FDM solution as the reference benchmark. The results demonstrate that incorporating a dynamic mesh refinement strategy significantly improves the performance of the PINN framework. In particular, the refined PINN achieves faster convergence, reaching a minimum loss of the order of 10^{-6} within substantially fewer iterations compared to the standard PINN. The improvement is further reflected in the predicted solution profiles, where the refined PINN exhibits excellent agreement with the FDM reference across multiple time instances. The absolute error analysis confirms this trend, showing that the refined model consistently attains lower error magnitudes throughout the spatio-temporal domain.

These findings highlight the effectiveness of directing collocation points toward high-residual regions, enabling the network to better capture sharp gradients and dynamic flow structures characteristic of the Shallow Water Equations. The dynamic mesh refinement strategy enhances numerical stability, accelerates optimisation, and increases predictive fidelity, making it a promising extension for physics-informed learning of non-linear and hyperbolic partial differential equations. Future research may explore the integration of real bathymetry data, variable bottom topography, and more complex boundary conditions, as well as extending the refinement strategy to higher-dimensional or coupled geophysical flow systems.

Acknowledgements

This research is funded through Universiti Malaysia Terengganu and Universitas Ahmad Dahlan under the International Partnership Research Grant (IPRG), Vot No.: 55382.

Conflict of Interest Statement

The authors confirm that no conflicts of interest arose at any stage in relation to the research findings presented.

References

[1] Bihlo, A., & Popovych, R. O. (2022). Physics-informed neural networks for the shallow-water equations on the sphere. *Journal of Computational Physics*, *456*, Article 111024.

[2] Cai, S., Wang, Z., Wang, S., Perdikaris, P., & Karniadakis, G. E. (2021). Physics-informed neural networks for heat transfer problems. *Journal of Heat Transfer*, *143*(6), Article 060801.

[3] Cuomo, S., Di Cola, V. S., Giampaolo, F., Rozza, G., Raissi, M., & Piccialli, F. (2022). Scientific machine learning through physics-informed neural networks: Where we are and what's next. *Journal of Scientific Computing*, *92*(3), Article 88.

[4] Farea, A., Yli-Harja, O., & Emmert-Streib, F. (2024). Understanding physics-informed neural networks: Techniques, applications, trends, and challenges. *AI*, *5*(3), 1534–1557.

[5] Gross, C., & Iwen, M. (2025). Sparse spectral methods for solving high-dimensional and multiscale elliptic PDEs. *Foundations of Computational Mathematics*, *25*(3), 765–811.

[6] Guo, J., Wang, H., Gu, S., & Hou, C. (2024). TCAS-PINN: Physics-informed neural networks with a novel temporal causality-based adaptive sampling method. *Chinese Physics B*, *33*(5), Article 050701.

[7] Irsalinda, N., Bakar, M. A., Harun, F. N., Surono, S., & Pratama, D. A. (2025). A new hybrid approach for solving partial differential equations: Combining physics-informed neural networks with cat-and-mouse based optimization. *Results in Applied Mathematics*, *25*, Article 100539.

[8] Jafarzadegan, K., Moradkhani, H., Pappenberger, F., Moftakhari, H., Bates, P., Abbaszadeh, P., & Duan, Q. (2023). Recent advances and new frontiers in riverine and

coastal flood modeling. *Reviews of Geophysics*, *61*(2). https://doi.org/10.1029/2022RG000788

[9] Li, P. W., Fan, C. M., & Grabski, J. K. (2021). A meshless generalized finite difference method for solving shallow water equations with the flux limiter technique. *Engineering Analysis with Boundary Elements*, *131*, 159–173.

[10] Luo, K., Zhao, J., Wang, Y., Li, J., Wen, J., Liang, J., & Liao, S. (2025). Physics-informed neural networks for PDE problems: A comprehensive review. *Artificial Intelligence Review*, *58*(10), 1–43.

[11] Lyu, C., Masson, Y., Romanowicz, B., & Zhao, L. (2024). Introduction to the distributional finite difference method for 3D seismic wave propagation and comparison with the spectral element method. *Journal of Geophysical Research: Solid Earth*, *129*(4), Article e2023JB027576.

[12] Naser, M. Z., & Alavi, A. H. (2023). Error metrics and performance fitness indicators for artificial intelligence and machine learning in engineering and sciences. *Architecture, Structures and Construction*, *3*(4), 499–517.

[13] Nath, D., Neog, D. R., & Gautam, S. S. (2024). Application of machine learning and deep learning in finite element analysis: A comprehensive review. *Archives of Computational Methods in Engineering*, *31*(5). https://doi.org/10.1007/s11831-024-10063-0

[14] Pratama, D. A., Abo-Alsabeh, R. R., Bakar, M. A., Salhi, A., & Ibrahim, N. F. (2023). Solving partial differential equations with hybridized physic-informed neural network and optimization approach: Incorporating genetic algorithms and L-BFGS for improved accuracy. *Alexandria Engineering Journal*, *77*, 205–226.

[15] Raissi, M., Perdikaris, P., & Karniadakis, G. E. (2017). Physics informed deep learning (part I): Data-driven solutions of nonlinear partial differential equations. *arXiv*. https://arxiv.org/abs/1711.10561

[16] Raissi, M., Perdikaris, P., Ahmadi, N., & Karniadakis, G. E. (2024). Physics-informed neural networks and extensions. *arXiv*. https://arxiv.org/abs/2408.16806

[17] Wang, W., Zhang, H., Zhou, Z., & Yang, X. (2024). A fast compact finite difference scheme for the fourth-order diffusion-wave equation. *International Journal of Computer Mathematics*, *101*(2), 170–193.

[18] Zaniboni, F., Zanuttigh, B., Istrati, D., & Armigliato, A. (2025). Coastal flood: From modelling to risk assessment and mitigation. In *Geohazards and disasters* (pp. 131–155). https://doi.org/10.1111/jfr3.12204

[19] Zhao, H., Hao, Y., Xu, W., & Li, C. (2024). Adaptive-sampling physics-informed neural network for viscoacoustic wavefield simulation. *IEEE Geoscience and Remote Sensing Letters*, *21*, 1–5.